World Journal of Gastroenterology

Submit a Manuscript: https://www.f6publishing.com

World J Gastroenterol 2024 April 21; 30(15): 2128-2142

DOI: 10.3748/wjg.v30.i15.2128

ISSN 1007-9327 (print) ISSN 2219-2840 (online)

ORIGINAL ARTICLE

Retrospective Study

Computed tomography-based radiomics to predict early recurrence of hepatocellular carcinoma post-hepatectomy in patients background on cirrhosis

Gui-Xiang Qian, Zi-Ling Xu, Yong-Hai Li, Jian-Lin Lu, Xiang-Yi Bu, Ming-Tong Wei, Wei-Dong Jia

Specialty type: Gastroenterology and hepatology

Provenance and peer review: Unsolicited article; Externally peer reviewed.

Peer-review model: Single blind

Peer-review report's scientific quality classification

Grade A (Excellent): 0
Grade B (Very good): 0
Grade C (Good): C
Grade D (Fair): 0
Grade E (Poor): 0

P-Reviewer: Abdelmoteleb M, Egypt

Received: December 30, 2023
Peer-review started: December 30, 2023
First decision: January 27, 2024
Revised: February 8, 2024
Accepted: March 12, 2024
Article in press: March 12, 2024
Published online: April 21, 2024

Gui-Xiang Qian, Xiang-Yi Bu, Wei-Dong Jia, Department of Hepatic Surgery, Anhui Provincial Hospital, The First Affiliated Hospital of USTC, Division of Life Science and Medicine, University of Science and Technology of China, Hefei 230001, Anhui Province, China

Zi-Ling Xu, Jian-Lin Lu, Ming-Tong Wei, Department of Hepatic Surgery, Anhui Provincial Hospital Affiliated to Anhui Medical University, Anhui Medical University, Hefei 230001, Anhui Province, China

Yong-Hai Li, Department of Anorectal Surgery, the First People's Hospital of Hefei, Hefei 230001, Anhui Province, China

Corresponding author: Wei-Dong Jia, PhD, Doctor, Department of Hepatic Surgery, Anhui Provincial Hospital, The First Affiliated Hospital of USTC, Division of Life Science and Medicine, University of Science and Technology of China, No. 17 Lujiang Road, Hefei 230001, Anhui Province, China. jwd1968@ustc.edu.cn

Abstract

BACKGROUND

The prognosis for hepatocellular carcinoma (HCC) in the presence of cirrhosis is unfavourable, primarily attributable to the high incidence of recurrence.

AIM

To develop a machine learning model for predicting early recurrence (ER) of post-hepatectomy HCC in patients with cirrhosis and to stratify patients' overall survival (OS) based on the predicted risk of recurrence.

METHODS

In this retrospective study, 214 HCC patients with cirrhosis who underwent curative hepatectomy were examined. Radiomics feature selection was conducted using the least absolute shrinkage and selection operator and recursive feature elimination methods. Clinical-radiologic features were selected through univariate and multivariate logistic regression analyses. Five machine learning methods were used for model comparison, aiming to identify the optimal model. The model's performance was evaluated using the receiver operating characteristic curve [area under the curve (AUC)], calibration, and decision curve analysis. Additionally, the Kaplan-Meier (K-M) curve was used to evaluate the strati-

fication effect of the model on patient OS.

RESULTS

Within this study, the most effective predictive performance for ER of post-hepatectomy HCC in the background of cirrhosis was demonstrated by a model that integrated radiomics features and clinical-radiologic features. In the training cohort, this model attained an AUC of 0.844, while in the validation cohort, it achieved a value of 0.790. The K-M curves illustrated that the combined model not only facilitated risk stratification but also exhibited significant discriminatory ability concerning patients' OS.

CONCLUSION

The combined model, integrating both radiomics and clinical-radiologic characteristics, exhibited excellent performance in HCC with cirrhosis. The K-M curves assessing OS revealed statistically significant differences.

Key Words: Machine learning; Radiomics; Hepatocellular carcinoma; Cirrhosis; Early recurrence; Overall survival; Computed tomography; Prognosis; Risk factor; Delta-radiomics

Core Tip: Hepatocellular carcinoma (HCC) ranks as the sixth most prevalent tumour and stands as the third leading cause of cancer-related deaths globally. In contrast to individuals with HCC in normal liver tissue, those with HCC in the context of cirrhosis frequently experience a higher recurrence rate. Therefore, a machine learning model aimed at predicting the early recurrence of post-hepatectomy HCC in patients with cirrhosis was developed. The study also aimed to stratify patients' overall survival based on the predicted risk of recurrence.

Citation: Qian GX, Xu ZL, Li YH, Lu JL, Bu XY, Wei MT, Jia WD. Computed tomography-based radiomics to predict early recurrence of hepatocellular carcinoma post-hepatectomy in patients background on cirrhosis. *World J Gastroenterol* 2024; 30(15): 2128-2142

URL: https://www.wjgnet.com/1007-9327/full/v30/i15/2128.htm

DOI: https://dx.doi.org/10.3748/wjg.v30.i15.2128

INTRODUCTION

Hepatocellular carcinoma (HCC) stands as the sixth most prevalent tumour and the third leading cause of cancer-related deaths globally[1]. Liver cirrhosis constitutes the primary risk factor for HCC, affecting nearly 90% of patients with HCC to varying degrees[1,2]. Curative-intent hepatectomy remains the preferred treatment for patients with early HCC[3]. However, the recurrence rate among patients with HCC surpasses 50%, significantly reducing long-term survival rates after resection[4]. The heightened risk of recurrence after curative-intent hepatectomy can be attributed to two patterns: recurrence stemming from residual microvascular metastasis after liver resection and recurrence due to the underlying liver carcinogenicity background[5]. Compared to patients with HCC in normal liver tissue, those with cirrhosis background HCC tend to experience both modes of recurrence, resulting in a higher recurrence rate after resection. Sasaki *et al*[6] observed a consistently higher risk of recurrence in the early postoperative period among patients with cirrhosis, with a 6% higher annual risk compared to non-cirrhotic resection for HCC (15%). Numerous staging systems, such as the Barcelona Clinic Liver Cancer staging system and the albumin-bilirubin grade, have been introduced for assessing the prognosis of patients with HCC[7]. However, these staging systems are more suited for evaluating liver function or guiding therapy. Given the high heterogeneity of HCC, patients with HCC during the same period might exhibit varying prognoses[8]. Currently, there is a lack of individualised prognosis assessment for patients, emphasising the crucial need for systematic surveillance of HCC recurrence and the accurate prediction of recurrence in patients with HCC.

In recent years, numerous studies have confirmed the impact of the inflammatory status within the tumour microenvironment on the occurrence and progression of tumours. However, the invasive nature of diagnosing these biomarkers, with associated risks of tumour seeding, bleeding, and sampling errors, has led to current guidelines not recommending biopsy diagnosis for HCC[9]. Therefore, there is a critical need for a non-invasive HCC marker to predict the early recurrence (ER) of HCC. Radiomics, a technique involving the extraction of quantitative image features through non-invasive, high-throughput analysis of standard medical imaging, presents a promising avenue. This method enables the extraction of data, which can be applied to enhance the accuracy of diagnostic, prognostic, and predictive assessments, ultimately serving as a bridge between medical imaging and individualised medical treatment[10,11]. The specific study flow of radiomics is illustrated in Figure 1.

Delta-radiomics involves extracting radiomics features from the same region of interest in a given patient to examine changes in radiomics characteristics over time. Unlike traditional radiomics methods that use single-phase images for feature extraction, which overlooks the image feature changes induced by alterations in blood flow after the introduction of a contrast agent, delta-radiomics offers a more comprehensive reflection of changes in pathological tissue or blood flow

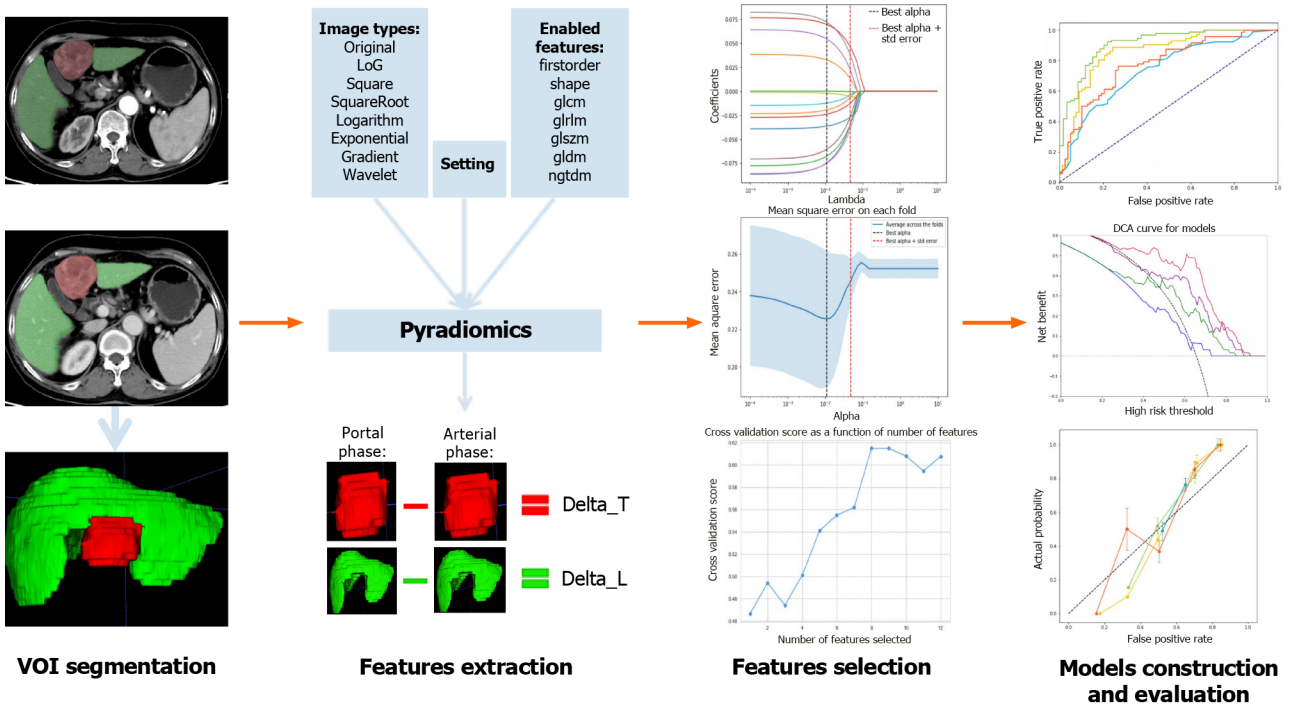

Figure 1 The workflow of radiomics, including volume of interest delineation, feature extraction, feature selection, and model building and evaluation. VOI: Volume of interest.

over time. This is particularly evident in patients with cirrhosis, where the pathophysiological conditions involve microvascular short-circuiting, compression of portal vein branches and hepatic veins by new modules, and disordered arrangement of hepatocyte cords[12]. In patients with cirrhosis, the liver buffer effect is continuously activated, resulting in compensatory arterial blood flow while the portal blood flow is reduced[13]. Delta-radiomics, by integrating the temporal component and radiomics features, provides additional insights into the evolution of feature values. The fixed time intervals of enhanced computed tomography (CT) images obtained during the arterial and portal phases lay the foundation for establishing delta-radiomics. Delta-radiomics features exhibit potential in diagnosing, prognosing, and predicting the therapeutic effects of certain tumours[14,15]. Han *et al*[16] used delta-radiomics features to predict the main pathological response of patients with non-small cell lung cancer to neoadjuvant chemotherapy and immunotherapy. The results indicated that the model formed by delta-radiomics features outperformed the single radiomics model. Based on the delta-radiomics model comprising eight features, Han *et al*[17] achieved an area under the curve (AUC) of 0.805 and 0.857 in the training and validation cohorts, respectively.

Several prior studies have explored the correlation between radiomics and HCC ER after curative-intent hepatectomy [18-22]. It is essential to note that these previous studies focussed solely on extracting radiomics features from tumours and peritumoural tissues. However, this study specifically addresses the background of cirrhosis, where the degree of cirrhosis in the remaining liver parenchyma varies subtly among different patients. Consequently, the analysis of radiomics characteristics encompasses not only the tumour tissue but also the residual liver tissue in this study.

This study aims to develop a machine learning model for predicting ER in HCC patients with cirrhosis. Additionally, the study aimed to assess whether the predicted outcomes of the model could accurately stratify patient overall survival (OS).

MATERIALS AND METHODS

This retrospective study was approved by the Institutional Review Board of our institution (2021-RE-043), and the need for written informed consent was waived.

Clinical information

From January 2014 to June 2020, 563 patients underwent hepatectomy for HCC at the First Affiliated Hospital of the University of Science and Technology of China (Anhui Provincial Hospital). Personal information, clinical information, and imaging features were retrospectively collected. The clinical index data and personal information, encompassing age and sex, for all included participants, were retrieved from the electronic medical records using the hospital system and the corresponding patient hospitalisation number.

HCC diagnosis was confirmed by postoperative pathology. The diagnosis of cirrhosis was based on clinical symptoms, laboratory tests, and imaging examinations, identifying compensated cirrhosis[23]. Curative resection was defined as the complete removal of all detectable tumour nodules by preoperative imaging and intraoperative exploration. This includes

criteria such as negative liver margin pathology, the absence of gross vascular and biliary invasion, no lymph node or extrahepatic distant metastasis, and, for most serum alpha-fetoprotein (AFP) positive patients, normalisation of marker levels within 2 months after surgery, coupled with imaging showing no new tumours. The exclusion criteria were as follows: (1) Non-cirrhotic patients; (2) tumours with extrahepatic metastasis or invasion of major blood vessels; (3) inability to obtain complete enhanced CT images or preoperative enhanced CT within a month; and (4) patients who underwent preoperative treatments such as partial hepatic resection, ablation, transarterial chemoembolisation, and other interventions. A total of 214 eligible patients were included in the study, and they were randomly assigned in a 7:3 ratio to the training cohort (150 patients) and the validation cohort (64 patients). The specific workflow is depicted in Figure 2.

CT equipment

All imaging procedures were performed using the GE Discovery HD 750 multi-row spiral CT scanner. Initially, a routine plain abdominal CT scan was performed on all patients to assess the extent of the lesions. During the scanning process, the abdominal CT parameters, including voltage, current, scanning layer thickness, layer spacing, and pixel matrix size, were set at 120 kV, 200-350 mA, 5 mm, 5 mm, and 512 × 512, respectively. After the non-enhanced CT scan, each patient received a non-ionic iodine contrast injection at a rate of 3.0 mL/s with a dose of 1.5 mL/kg. The arterial phase scan commenced 35 s after the density of the descending aorta reached 95 HU, followed by the initiation of the portal phase scan 35 s after the arterial phase scan.

Imaging information

Digital imaging and communications in medicine-formatted CT images of all patients were retrieved from the hospital picture archiving and communication system. During the assessment, two readers, each possessing extensive experience in liver imaging (Xu ZL and Lu JL), independently recorded nine semantic features: Non-peripheral washout, maximum tumour diameter, tumour capsule, intratumour vascularity, tumour growth pattern, fusion lesions, intratumour necrosis, peritumoural enhancement, and arterial phase hyperenhancement. Simultaneously, the three-dimensional volume algorithm was employed to calculate the tumour volume. In cases where multiple lesions were present in the patient's liver, the tumour with the maximum diameter was selected as the subject for evaluation. To provide a more visual understanding of these imaging semantic features, reference images are included for illustration (Figure 3).

Follow-up

All discharged patients were subjected to regular follow-ups, encompassing monitoring of serum AFP levels, liver function tests, and abdominal ultrasound within the first month after curative liver resection. Subsequent evaluations for HCC recurrence occurred every 3 or 6 months thereafter. In cases where an unexplained elevation in serum AFP levels or abnormal abdominal ultrasound or enhanced ultrasound findings were observed during follow-up, further assessment was performed through dynamic contrast-enhanced CT or magnetic resonance imaging. Recurrence-free survival was defined as the duration from the date of surgery to the first recurrence, metastasis, or the last follow-up. OS was defined as the time from the date of surgery to death from any cause. The study was reviewed on 31 August 2023.

Image segmentation and feature extraction

The volume of interest (VOI) was defined as the entire tumour or the residual liver, excluding peritumoural vessels or bile ducts. Two readers, Xu ZL and Lu JL, blinded to patient outcomes, delineated the patients' VOI layer by layer using ITK-SNAP (v3.6). To ensure the stability of the extracted features, the interobserver reproducibility of the extracted features between the two readers was evaluated. Subsequently, images from 40 cases in the derivation cohort were randomly selected, and the same segmentation procedure was repeated a month later by the same two radiologists to evaluate intraobserver reproducibility. Interobserver reproducibility was evaluated by calculating the intraclass correlation coefficient (ICC).

The Pyradiomics (v3.1.0) software package in Python (v3.8.4) was used for the extraction of radiomics features. To ensure the reproducibility of the extracted features, standardised calculations of radiomics features were used. Within the Pyradiomics package, the following steps were executed: Considering our hospital's machine had a sampling layer thickness of 5 mm, resampling was performed only for the coronal and sagittal positions, with a resampling size of 1 mm × 1 mm × 5 mm. In terms of image types, the original, square, square root, logarithm, exponential, gradient, Laplacian of Gaussian filter, and wavelet filters were applied to the original image.

The extracted features were classified into seven distinct types: (1) Shape; (2) first-order statistics; (3) grey level co-occurrence matrix; (4) grey level run length matrix; (5) grey level size zone matrix; (6) neighbouring grey tone difference matrix; and (7) grey level dependence matrix. After excluding features that could not be analysed, each patient yielded six groups of features, including tumour and residual liver during the arterial and portal phases, along with delta-radiomics (representing the difference between the tumour and residual liver in the portal and arterial phases). This resulted in 1512 features within each group.

Radiomics and clinical-radiologic feature statistics

Given the substantial number of features and their high dimensions, complete inclusion in the model might increase the risk of overfitting. To mitigate this and enhance generalisation, a three-step feature screening method was implemented. First, features with an ICC of < 0.8 were excluded. Subsequently, the selected features underwent Z-score standardisation and were subjected to the least absolute shrinkage and selection operator (LASSO) fitting. To prevent overfitting resulting from an excessive number of features after LASSO, if the number of features after remained > 1, a decision tree classifier was employed as the kernel, and recursive feature elimination was applied to determine the optimal number of features

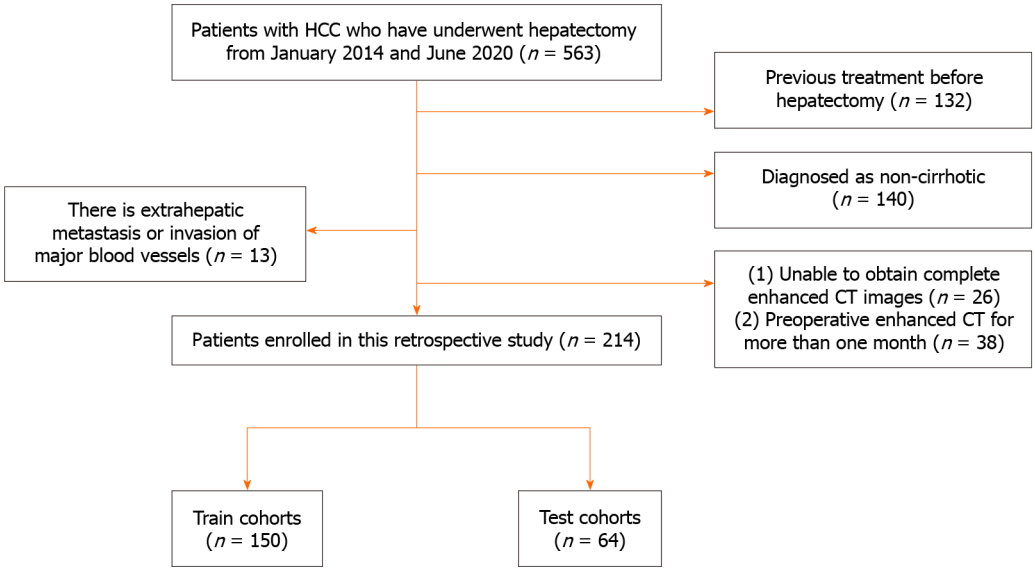

Figure 2 Flowchart illustrating the inclusion and exclusion of patients. HCC: Hepatocellular carcinoma; CT: Computed tomography.

in each group. This screening process was iteratively conducted for each feature group to acquire more representative features. Ultimately, the Rad-score was computed based on the feature-weighted regression coefficient derived from LASSO.

R software (v4.3.0) was employed for analysing clinical-radiologic data. Continuous data were subjected to the *t*-test, and their distribution is presented as the mean ± SD. Categorical data underwent analysis using the chi-square test or Fisher's exact test, and the results are presented as percentages. In the univariate analysis, variables with a P value of < 0.05 were selected and subsequently included in the multivariable logistic regression model for further analysis. All statistical tests were two-sided, with statistical significance set at $P < 0.05$.

Machine learning model building

To minimise discrepancies arising from varying optimal models for different features, this study did not adhere to a fixed model. Instead, the best model was chosen based on the data of each feature, followed by a comparison of the final results. The training cohort was used to identify optimal parameters and develop the prediction model, while the validation cohort was employed to assess prediction performance. The radiomics model was constructed using the scikit-learn (v1.0.2) package in Python, including Support Vector Machine (SVM), Random Forest, K-Nearest Neighbour (KNN), Light Gradient-boosting Machine, and eXtreme Gradient Boosting. A five-fold cross-validation was performed on the training cohort, and the average AUC was calculated. To prevent overfitting and underfitting, models were excluded if their average AUC in the training cohort exceeded or fell below 10% of that in the validation cohort. Subsequently, the AUC of the validation cohort was calculated to evaluate model performance, and the best-selected model was used for the subsequent comparison.

RESULTS

Patient baseline characteristics

This study included 214 patients, among which 114 experienced ER. For model development, 150 patients were randomly assigned to the training cohort. The baseline values of clinical-radiologic characteristics for the training and validation cohorts are presented in Table 1, and no significant differences were observed between the characteristics of the two cohorts ($P > 0.05$). The results of the univariate and multivariate analyses are presented in Table 2, revealing that the final three clinical-radiologic features, namely, gamma-glutamyl transferase (GGT), tumour capsule, and peritumoural enhancement, were included in the subsequent analysis.

Feature selection

To evaluate the characteristics of ER of HCC with cirrhosis, each patient's six feature groups included the following: Arterial phase tumours (A1), arterial phase liver (A2), portal phase tumour (P1), portal phase liver (P2), the characteristic difference between portal and arterial phase tumour (delta-T), and the difference between portal and arterial liver (delta-L). After the feature selecting step, two features were obtained in A1, one feature in A2, three features in P1, three features in P2, and three delta-radiomics (comprising two features in delta-T and one feature in delta-L). In total, 12 features were extracted from the six groups.

Table 1 The clinical-radiologic characteristics of primary cohort, *n* (%)

Variable	Training cohort (*n* = 150)	Validation cohort (*n* = 64)	*P* value
Tumor-volume (cm^3), mean ± SD	249 ± 381	318 ± 361	0.219
Age (yr), mean ± SD	57.3 ± 10.1	54.5 ± 11.7	0.079
Rad-score	0.4 ± 0.2	0.52 ± 0.16	0.121
BMI			0.691
0, < 18.5	7 (4.67)	3 (4.69)	
1, 18.5-25	109 (72.7)	43 (67.2)	
2, ≥ 25	34 (22.7)	18 (28.1)	
AFP (ng/mL)			0.382
0, ≤ 400	91 (60.7)	34 (53.1)	
1, > 400	59 (39.3)	30 (46.9)	
sex			0.839
0, male	128 (85.3)	56 (87.5)	
1, female	22 (14.7)	8 (12.5)	
Hepatitis (HBV/HCV)			0.407
0, absent	22 (14.7)	6 (34.4)	
1, present	128 (85.3)	58 (90.6)	
N (× 10^9/L)			0.275
0, < 1.8	127 (84.7)	54 (84.4)	
1, 1.8-6.3	18 (12.0)	10 (15.6)	
2, > 6.3	5 (3.33)	0 (0.00)	
L (× 10^9/L)			0.504
0, ≥ 1.1	119 (79.3)	54 (84.4)	
1, < 1.1	31 (20.7)	10 (15.6)	
PLT (× 10^9/L)			0.703
0, > 100	120 (80.0)	49 (76.6)	
1, ≤ 100	30 (20.0)	15 (23.4)	
ALT (U/L)			0.959
0, ≤ 50	117 (78.0)	49 (76.6)	
1, > 50	33 (22.0)	15 (23.4)	
AST (U/L)			0.854
0, > 40	67 (44.7)	27 (39.1)	
1, ≤ 40	83 (55.3)	39 (60.9)	
GGT (U/L)			0.113
0, ≤ 60	78 (52.0)	25 (43.8)	
1, > 60	72 (48.0)	39 (56.2)	
TB (umol/L)			0.605
0, ≤ 21	110 (73.3)	44 (68.8)	
1, > 21	40 (26.7)	20 (31.2)	
ALB (g/L)			0.720
0, ≤ 40	76 (50.7)	30 (46.9)	
1, > 40	74 (49.3)	34 (53.1)	

NLR			0.697
0, ≤ 2	74 (49.3)	29 (45.3)	
1, > 2	76 (50.7)	35 (54.7)	
PLR			0.528
0, ≥ 95	78 (52.0)	37 (57.8)	
1, < 95	72 (48.0)	27 (42.2)	
HbsAg			1
Negative	18 (12.0)	8 (12.5)	
Positive	132 (88.0)	56 (87.5)	
BCLC			0.554
0, stage0	7 (4.67)	5 (7.81)	
1, stageA	143 (95.3)	59 (92.2)	
CNLC			0.308
0, Ia	74 (49.3)	26 (40.6)	
1, Ib	76 (50.7)	38 (59.4)	
Non-peripheral washout			0.738
0, absent	2 (1.33)	2 (3.12)	
1, present	148 (98.7)	62 (96.9)	
Tumor capsule			0.110
0, ill-defined capsule	58 (38.7)	33 (51.6)	
1, well-defined capsule	92 (61.3)	31 (48.4)	
Intratumor vascularity			0.654
0, absent	24 (16.0)	8 (12.5)	
1, present	126 (84.0)	56 (87.5)	
Tumor growth pattern			0.635
0, intrahepatic growth	56 (37.3)	21 (32.8)	
1, extrahepatic growth	94 (62.7)	43 (67.2)	
Fusion lesions			0.255
0, absent	87 (58.0)	31 (48.4)	
1, present	63 (42.0)	33 (51.6)	
Intratumor necrosis			0.05
0, absent	47 (31.3)	11 (17.2)	
1, present	103 (68.7)	53 (82.8)	
Peritumoral enhancement			1
0, absent	90 (60.0)	39 (60.9)	
1, present	60 (40.0)	25 (39.1)	
Tumor margin			0.76
0, smooth	84 (56.0)	38 (59.4)	
1, non-smooth	66 (44.0)	26 (40.6)	
Arterial phase hyperenhancement			0.738
0, absent	2 (1.33)	2 (3.12)	
1, present	148 (98.7)	62 (96.9)	

BMI: Body mass index; AFP: Alpha fetoprotein; N: Neutrophil; L: Lymphocyte; ALT: Alanine transferase; AST: Aspartate transferase; GGT: Gamma-glutamyl transferase; PLT: Platelets; TB: Total bilirubin; ALB: Albumin; NLR: Neutrophil-to-lymphocyte ratio; PLR: Platelet-to-lymphocyte ratio; BCLC: Barcelona Clinic Liver Cancer; CNLC: China Liver Cancer Staging System.

Table 2 Of 150 patients univariate and multivariate logistic regression analysis

Variable	Univariable			Multivariable		
	OR	95%CI	*P* value	OR	95%CI	*P* value
Tumor-volume	1.00	1.00-1.00	0.022	1.00	1.00-1.00	0.189
Rad-score	238.02	20.57-2754.04	0.001	298.44	12.57-7083.67	< 0.001
AST						
0, > 40						
1, ≤ 40	0.47	0.25-0.91	0.025	0.93	0.38-2.29	0.875
GGT						
0, ≤ 60						
1, > 60	3.99	2.02-7.86	0.001	2.50	1.07-5.86	0.034
CNLC						
0, Ia						
1, Ib	2.26	1.17-4.35	0.015	1.02	0.39-2.63	0.975
Capsule appearance						
0, ill-defined						
1, well-defined capsule	0.44	0.23-0.86	0.017	0.33	0.14-0.77	0.01
Peritumoral enhancement						
0, absent						
1, present	3.21	1.62-6.34	0.001	3.85	1.67-8.88	0.002

AST: Aspartate transferase; GGT: Gamma-glutamyl transferase; CNLC: China Liver Cancer Staging System.

Model comparison

Initially, three models were developed based on the radiomics features. Model 1 comprised A1 and P1, Model 2 included A1, P1, A2, and P2, and Model 3 included A1, P1, A2, P2, and delta-radiomics. All three radiomics feature models employed SVM as the optimal machine learning method. The performance effects among the models are illustrated in Figure 4, with Model 3 achieving an AUC value of 0.756 in the validation cohort. Compared with Models 1 and 2 performance, our subsequent study opted for the radiomics features in Model 3. Furthermore, a combined model was established by integrating clinical-radiologic and radiomics features, which was compared with the clinical-radiologic model and the radiomics model. As shown in Table 3, the SVM emerged as the best model established by radiomics, while the KNN was the optimal model established by the clinical-radiologic and combined models.

Combined model construction and performance evaluation

The combined model, integrating both radiomics and clinical-radiologic features, demonstrated enhanced diagnostic and predictive efficacy, achieving an AUC of 0.844 in the training cohort and an AUC of 0.790 in the validation cohort. In contrast, the AUC for the clinical-radiologic model was 0.763 in the training cohort and 0.701 in the validation cohort. The AUC values for radiomics features were 0.726 and 0.756, respectively (Figure 5A and B). The Delong test, presented in Table 4, revealed the superiority of the combined model compared to the clinical-radiologic model. Both the calibration curve and the decision curve analysis curve illustrated the commendable calibration and clinical applicability of the combined model (Figure 5C-F). The optimal cut-off value, determined as the maximum Youden index (0.53) in the combined model training cohort, was applied to the training and validation cohorts. This facilitated the categorisation of patients into low-risk and high-risk groups, and the stratification results of patients' OS were analysed using the Kaplan-Meier (K-M) curve. The K-M curve shows that the optimal cut-off value successfully stratified patients OS (Figure 6).

Table 3 Comparison of machine learning model performance

	Models	Training cohort			Validation cohort		
		Accuracy	Precision	AUC	Accuracy	Precision	AUC
Cli	SVM	0.720	0.750	0.736	0.688	0.867	0.686
	RF	0.720	0.750	0.768	0.688	0.867	0.680
	KNN	0.693	0.667	0.763	0.672	0.756	0.701
	XGB	0.720	0.750	0.768	0.688	0.867	0.680
	LightGBM	0.720	0.750	0.761	0.688	0.867	0.693
Rad	SVM	0.673	0.695	0.726	0.719	0.853	0.756
	RF	0.753	0.761	0.849	0.672	0.744	0.688
	KNN	0.713	0.716	0.809	0.656	0.778	0.690
	XGBoost	0.860	0.849	0.945	0.594	0.700	0.588
	LightGBM	0.727	0.696	0.820	0.688	0.729	0.629
Con	SVM	0.727	0.754	0.778	0.688	0.867	0.739
	RF	0.727	0.731	0.820	0.797	0.872	0.777
	KNN	0.767	0.747	0.844	0.719	0.816	0.790
	XGB	0.840	0.875	0.924	0.609	0.743	0.656
	LightGBM	0.807	0.787	0.892	0.719	0.800	0.771

Five model performance evaluation results from clinical-radiologic, radiomics andcombined models. Cli: Clinical-radiologic model; Rad: Radiomics model; Con: Combined model.

Table 4 Delong test between models

Model	Model	Train		Validation	
		Z	*P* value	Z	*P* value
Cli	Rad	0.757	0.449	-0.791	0.429
Cli	Con	-2.988	0.003	-2.099	0.036
Rad	Con	-3.253	0.001	-0.713	0.476

Cli: Clinical-radiologic model, Rad: Radiomics model, Con: Combined model.

DISCUSSION

HCC is characterised by considerable heterogeneity, and the status of ER in HCC significantly influences the OS. HCC associated with cirrhosis exhibits a higher recurrence rate compared to HCC arising in an individual with a normal hepatic background, thereby contributing to diminished survival rates[6]. In our study, among the 214 patients, 114 patients experienced ER, constituting 53.3% of the total study population. Consequently, the imperative to develop models capable of predicting HCC ER before surgery is of great importance in clinical practice.

Our study revealed that tumour capsule, peritumoural enhancement, GGT, and Rad-score serve as predictors of ER in HCC within the context of cirrhosis. Employing the KNN algorithm, a combined model was established, establishing an AUC of 0.844 in the training cohort and 0.790 in the validation cohort. The Delong test revealed that the difference between the radiomics and clinical-radiologic models in the validation cohort lacked statistical significance, suggesting that the radiomics model can yield predictive results comparable to those of the clinical-radiologic model. Furthermore, the combined model outperformed the clinical-radiologic model in the training and validation cohorts, indicating the pivotal role of radiomics in predicting HCC within the context of liver cirrhosis (Table 4). For patient stratification, the maximum Youden index of the combined model was used as the optimal cut-off value (0.53), categorising patients into ER high-risk and low-risk groups. Subsequently, K-M curve analysis was employed to stratify patients' OS. The results demonstrated a significant difference in the OS between patients in ER high-risk and low-risk groups.

Previous studies have reported that peritumoural enhancement and tumour capsule are predictive factors for postoperative HCC recurrence[23-25]. This association might stem from the correlation between peritumoural en-

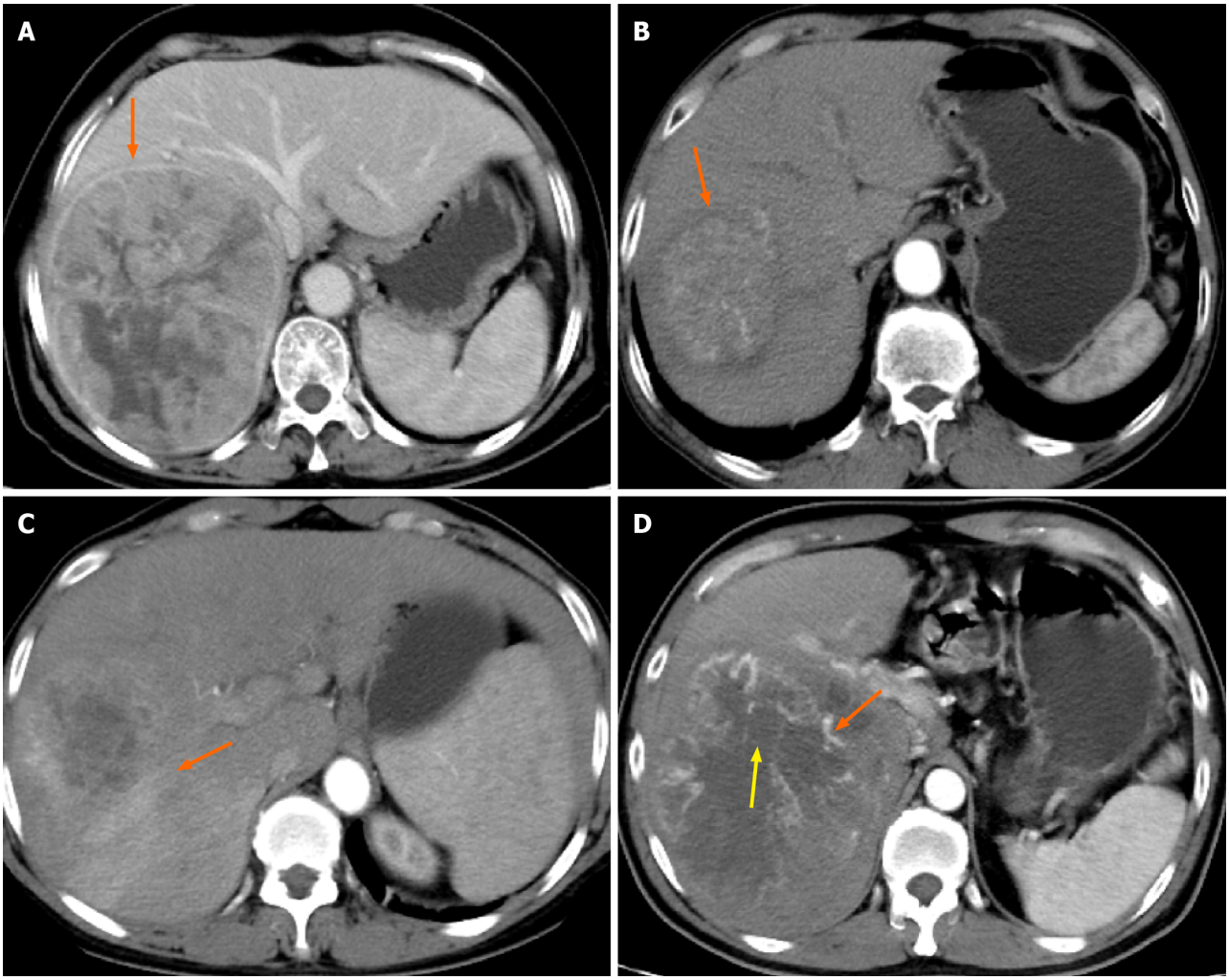

Figure 3 Example of the typical computed tomography images of the semantic features. A: The tumour capsule is observed in the direction indicated by the arrow, with a ring-like high-density appearance around the tumour in the portal phase; B: Smooth tumour margins are observed in the direction of arrows; C: Peritumoural enhancement is visible in the direction of the arrow, characterised by a patchy, high-density area outside the tumour range in the arterial phase; D: Intratumour necrosis within the tumour is observed in the direction of the red arrow, demonstrating a low-density area in the arterial phase. Additionally, the yellow arrow highlights intratumour vascularity, appearing as a linear high-density area within the arterial phase.

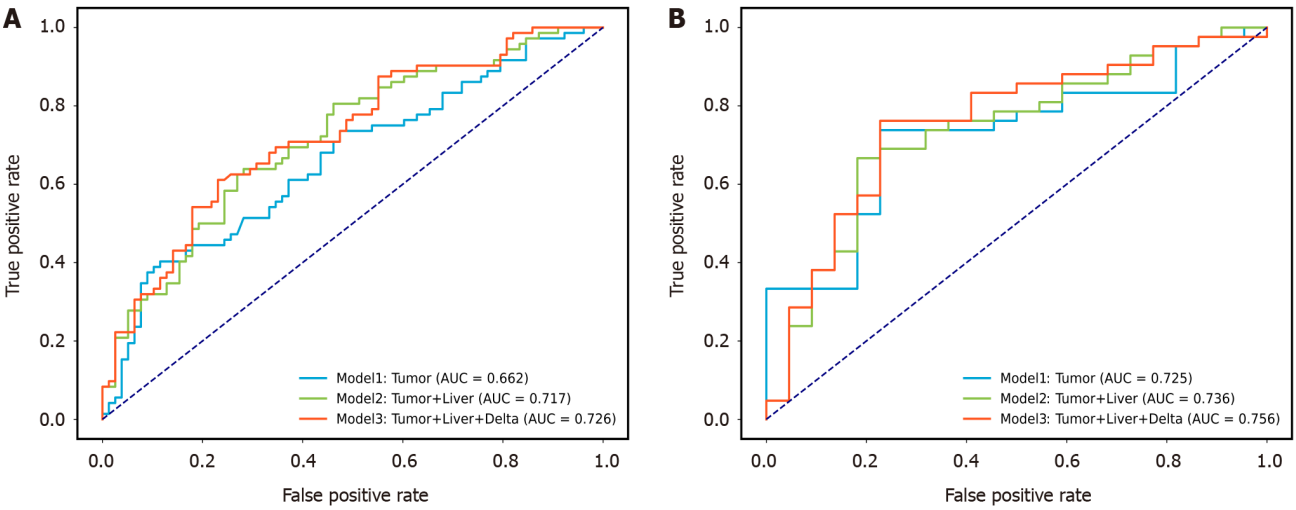

Figure 4 Receiver operating characteristic curve for three radiomics models developed using support vector machine. A: The performance of the three radiomics models in the training cohort; B: The performance of the three models in the validation cohort reveals that the area under the curve of Model 3 was 0.762, and its performance was better than that of Models 1 and 2. AUC: Area under the curve.

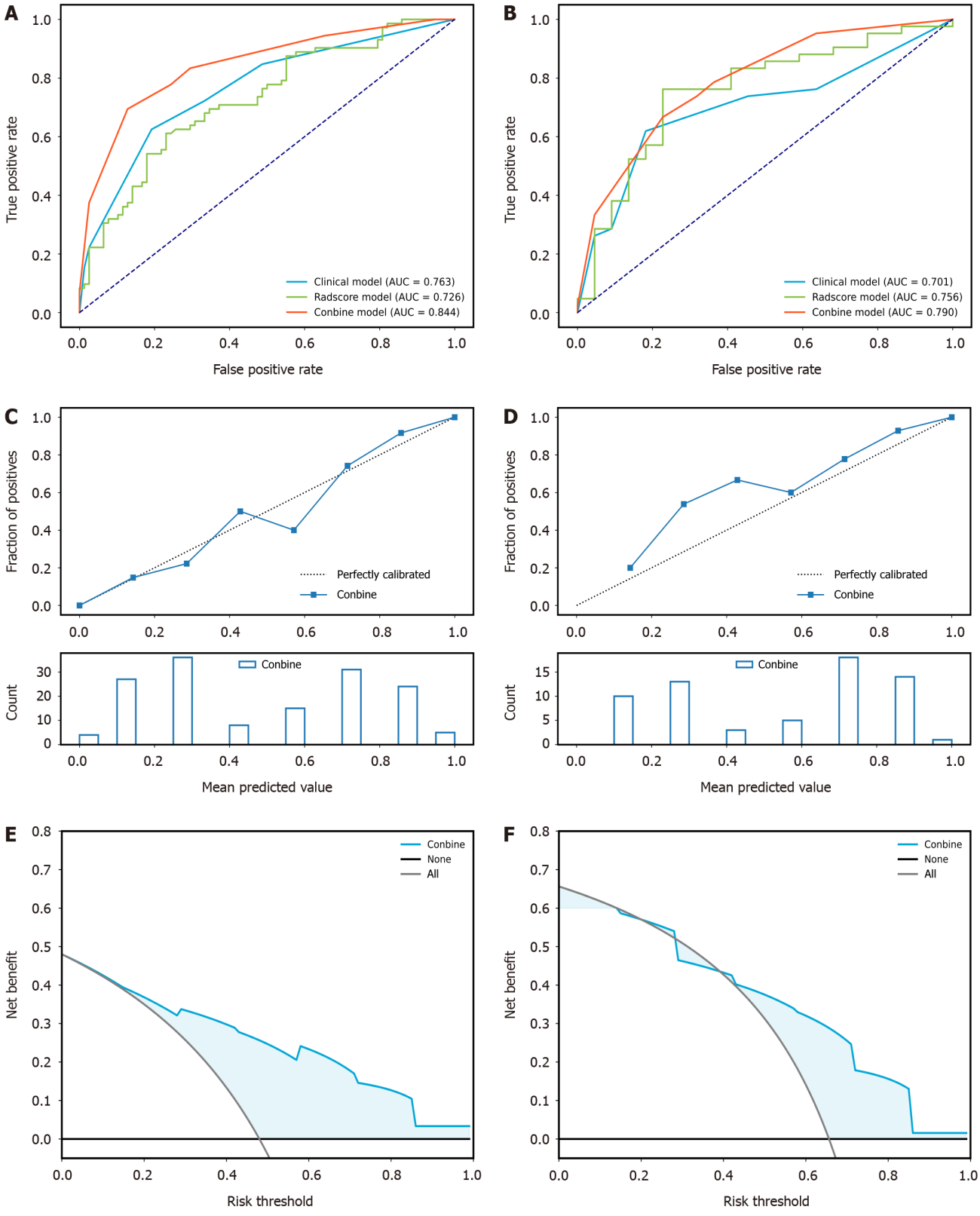

Figure 5 Receiver operating characteristic of the clinical-radiologic model established by K-Nearest Neighbour, radiomics model established by support vector machine, and the combined model established by K-Nearest Neighbour. A: The area under the curve (AUC) values of the clinical-radiologic, radiomics, and combined models in the training cohort were 0.763, 0.726, and 0.844, respectively; B: In the validation cohort, the AUC values of the clinical-radiologic, radiomics, and combined models were 0.701, 0.756, and 0.790, respectively; C: Calibration curve performance of the combined model in the training cohort; D: Combined model calibration curve in the validation cohort; E: Decision curve analysis (DCA) of the combined model in the training cohort; F: DCA of the combined model in the validation cohort. AUC: Area under the curve.

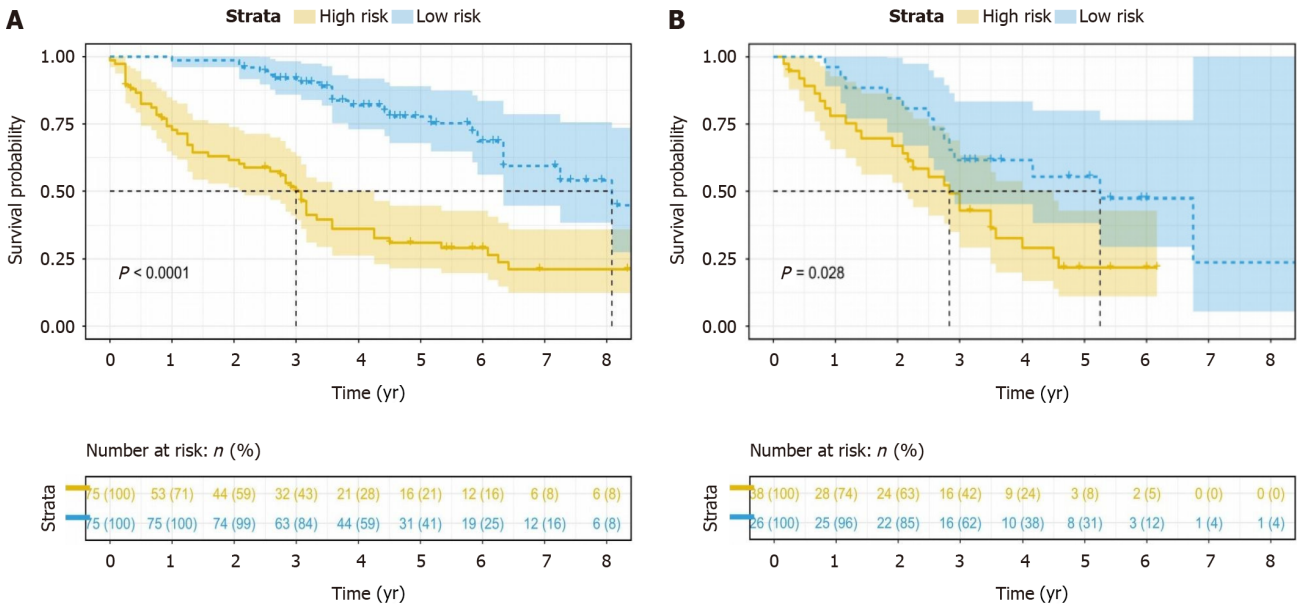

Figure 6 Kaplan-Meier curve analysis of the overall survival of patients stratified based on the best Youden index after hepatectomy. The high-risk and low-risk groups had scores > 0.53 and < 0.53, respectively. A: In the training cohort, the median overall survival (OS) was 3.00 and 8.08 years for the high-risk and low-risk groups, respectively ($P < 0.0001$); B: In the validation cohort, the median OS was 2.83 and 5.25 years for the high-risk and low-risk groups, respectively ($P = 0.028$).

hancement, tumour capsule, and microvascular invasion (MVI) in HCC[26]. Numerous studies have consistently identified MVI as an independent risk factor for ER and unfavourable prognosis after HCC surgery[27,28]. Additionally, GGT has been identified as a predictive factor for adverse outcomes after HCC[29,30]. Our study findings, indicating GGT, tumour capsule, and peritumoural enhancement as independent risk factors for ER of HCC, align with previous studies. However, predicting the ER of HCC solely based on clinical-radiologic factors remains suboptimal (AUC 0.701). Therefore, there is a need for a more precise and convenient method to predict patient outcomes. Radiomics, an emerging imaging analysis approach, uses data mining algorithms to extract features from existing medical images. Subsequently, statistical analysis tools are employed to analyse high-throughput imaging features, providing predictive or prognostic information[10]. Prior to this study, radiomics has been widely used for predicting the diagnosis and prognosis of HCC [31-33]. Notably, delta-radiomics has demonstrated the ability to establish models with high performance. In a study by Xia *et al*[34] a hybrid model combining clinical-radiologic features and delta-radiomics predicted MVI with AUC values of 0.86 and 0.84 in the internal and external validation cohorts, respectively. This model also effectively classified the ER-free rate and OS. Another study by Liu *et al*[35] developed a model based on the AP-TP 5 signal for OS in patients with HCC, achieving AUC values between 0.774-0.837 in the training cohort and 0.754-0.810 in the validation cohort for 1-3 year predictions. Unlike previous studies that primarily discussed the ER of HCC with cirrhosis, previous solely using clinical data[36], our study not only addressed this issue but also incorporated radiomics and compared it with clinical-radiologic features. Ultimately, a combined model with an AUC of 0.790 in the validation cohort was developed.

Past studies often compared clinical-radiologic models, radiomics models, and combined models using the same machine learning methods[37]. However, the optimal models corresponding to different features might vary. To address this issue, our study employed five different machine learning methods and compared the best models corresponding to each feature using specific algorithms, mitigating the bias introduced by different model selections. In this study, three models were compared: one only with tumour features (Model 1), another with tumour and residual liver features (Model 2), and a third with tumour, residual liver, and delta-radiomics features (Model 3). The results revealed the superior performance of Model 3, established with SVM. Simultaneously, this algorithm was used to compare the clinical-radiologic, radiomics, and combined models. The outcomes demonstrated that the combined model, established by KNN exhibited the best performance. This approach allows for a more accurate assessment of the various models' performance and enables the selection of the most suitable model for predicting the prognosis of HCC.

However, it is crucial to acknowledge certain limitations in our study. First, being a retrospective study, the possibility of selection bias could not be eliminated. Second, the study was conducted solely at a single centre, and conducting a multicentre validation study would enhance the reliability of the results. Therefore, it is expected that future studies will involve a multicentre prospective study to validate our findings. Third, the primary aetiology among patients with cirrhosis in our study was hepatitis B and C. Consequently, further verification of the model established by us is warranted in HCC patients with cirrhosis caused by other factors. Fourth, from a machine learning perspective, the sample size in this study is relatively small. Consequently, ongoing efforts will involve the inclusion of new samples to continually train and validate our model. Fifth, in our study, manual delineation was still employed, proving to be time-consuming and resource-intensive. Although attempts were made to employ deep learning networks for training tools to automatically segment the liver and tumour, the results were not sufficiently accurate, primarily due to the limitation of a small sample size. Moving forward, the plan is to expand the sample size to train a deep learning network model capable

of fully automating the segmentation of the patient's tumour and the residual liver.

CONCLUSION

In this study, the combined model for predicting the ER of HCC was constructed using KNN. The AUC values were 0.844 and 0.790 in the training and validation cohorts, respectively. The K-M curves demonstrated that the outcomes predicted by the combined model could correctly stratify patients' OS. The prospective application of this model in clinical practice holds promise for delivering precise, individualised guidance for patient prognosis.

ARTICLE HIGHLIGHTS

Research background

Hepatocellular carcinoma (HCC) ranks as the sixth most prevalent tumour and stands as the third leading cause of cancer-related deaths globally. Liver cirrhosis emerges as the primary risk factor for HCC, affecting nearly 90% of patients with HCC to varying degrees. The prognosis for HCC with cirrhosis remains poor, primarily attributable to the elevated recurrence rates.

Research motivation

Individuals with HCC in the background of cirrhosis frequently experience higher recurrence rates compared to patients with HCC in a non-cirrhotic liver. Therefore, the purpose of our study was to establish a model that could predict early recurrence (ER) of HCC within the context of cirrhosis.

Research objectives

To develop a machine learning model to predict the ER of post-hepatectomy HCC in patients with cirrhosis and stratify patients' overall survival (OS) based on the predicted risk of recurrence.

Research methods

In this retrospective study, 214 HCC patients with cirrhosis who underwent curative hepatectomy were examined. Radiomics feature selection employed the least absolute shrinkage and selection operator and recursive feature elimination. Clinical-radiologic features were selected through univariate and multivariate logistic regression analyses. Five machine learning methods were used for model comparison and optimal model selection. The area under the receiver operating characteristic curve (AUC), calibration, and decision curve analysis were used to evaluate the model's performance. The Kaplan-Meier (K-M) curve was used to assess the model's stratification effect on patient OS.

Research results

The optimal performance in predicting ER of HCC within the context of cirrhosis was observed in a model that integrated radiomics features and clinical-radiologic features. This model attained an AUC of 0.844 in the training cohort and 0.790 in the validation cohort. K-M curves demonstrated that the combined model not only allowed for risk stratification but also exhibited significant discrimination in patients' OS.

Research conclusions

The combined model that integrates radiomics and clinical-radiologic characteristics achieved excellent performance in patients with HCC with a background of cirrhosis. K-M curves assessing OS revealed statistically significant differences.

Research perspectives

Given the significant impact of ER on the prognosis of HCC in patients with cirrhosis, accurately predicting such recurrence is paramount. The study aims to investigate the prediction of ER in HCC with cirrhosis using enhanced computed tomography radiomics.

FOOTNOTES

Co-first authors: Gui-Xiang Qian and Zi-Ling Xu.

Author contributions: Qian GX and Jia WD designed the research study; Qian GX, Xu ZL, Li YH, Bo XY, Wei MT and Lu JL collected the data; Xu ZL, Lu JL and Wei MT analyzed the data; all authors wrote the manuscript; Qian GX, Li YH, and Jia WD revised the manuscript; all authors have read and approve the final manuscript. Qian GX and Xu ZL have made equivalent contributions in this article. The reasons are as follows: First, the research covered in this manuscript was a collaborative team effort, with each author dedicating substantial time and effort. Qian GX was responsible for study design, method development, data collection, experimental data analysis, manuscript writing, and subsequent revisions. Meanwhile, Xu ZL played a significant role in data collection, data analysis, and initial manuscript drafting. Second, Xu ZL brings valuable clinical experience to the team. Throughout the research collaboration

with Qian GX, Xu ZL continuously refined the study process, leveraging his accumulated knowledge to identify and rectify potential errors. On the other hand, Qian GX skillfully applied her clinical and machine learning expertise to ensure the study's quality and reliability. Given these reasons, and to accurately reflect the efforts and contributions of each author, I, as the corresponding author, have designated Qian GX and Xu ZL as co-first authors for this study, acknowledging their equal contributions.

Supported by Anhui Provincial Key Research and Development Plan, No. 202104j07020048.

Institutional review board statement: This study was reviewed and approved by the Ethics Committee of the First Affiliated Hospital of the University of Science and Technology of China (Anhui Provincial Hospital) (2021-RE-043).

Informed consent statement: The need for informed consent was waived owing to the retrospective nature of the study. All procedures involving human participants were in accordance with the Declaration of Helsinki and its subsequent amendments.

Conflict-of-interest statement: All authors declare that they have no conflict of interest.

Data sharing statement: The datasets generated and/or analysed during the current study are not publicly available due to patient privacy and copyright issues but are available from the corresponding author upon reasonable request.

Country/Territory of origin: China

ORCID number: Gui-Xiang Qian 0000-0002-3971-7258; Zi-Ling Xu 0009-0007-4487-9415; Yong-Hai Li 0009-0009-2777-1941; Jian-Lin Lu 0009-0009-4466-0565; Xiang-Yi Bu 0009-0001-6543-0066; Ming-Tong Wei 0009-0001-3894-4125; Wei-Dong Jia 0009-0008-1419-3401.

S-Editor: Qu XL
L-Editor: A
P-Editor: Yuan YY

REFERENCES

1 **Forner A**, Reig M, Bruix J. Hepatocellular carcinoma. *Lancet* 2018; **391**: 1301-1314 [PMID: 29307467 DOI: 10.1016/S0140-6736(18)30010-2]
2 **Ginès P**, Krag A, Abraldes JG, Solà E, Fabrellas N, Kamath PS. Liver cirrhosis. *Lancet* 2021; **398**: 1359-1376 [PMID: 34543610 DOI: 10.1016/S0140-6736(21)01374-X]
3 **European Association for the Study of the Liver**. EASL Clinical Practice Guidelines: Management of hepatocellular carcinoma. *J Hepatol* 2018; **69**: 182-236 [PMID: 29628281 DOI: 10.1016/j.jhep.2018.03.019]
4 **Tabrizian P**, Jibara G, Shrager B, Schwartz M, Roayaie S. Recurrence of hepatocellular cancer after resection: patterns, treatments, and prognosis. *Ann Surg* 2015; **261**: 947-955 [PMID: 25010665 DOI: 10.1097/SLA.0000000000000710]
5 **Imamura H**, Matsuyama Y, Tanaka E, Ohkubo T, Hasegawa K, Miyagawa S, Sugawara Y, Minagawa M, Takayama T, Kawasaki S, Makuuchi M. Risk factors contributing to early and late phase intrahepatic recurrence of hepatocellular carcinoma after hepatectomy. *J Hepatol* 2003; **38**: 200-207 [PMID: 12547409 DOI: 10.1016/s0168-8278(02)00360-4]
6 **Sasaki K**, Shindoh J, Margonis GA, Nishioka Y, Andreatos N, Sekine A, Hashimoto M, Pawlik TM. Effect of Background Liver Cirrhosis on Outcomes of Hepatectomy for Hepatocellular Carcinoma. *JAMA Surg* 2017; **152**: e165059 [PMID: 28052155 DOI: 10.1001/jamasurg.2016.5059]
7 **Toyoda H**, Lai PB, O'Beirne J, Chong CC, Berhane S, Reeves H, Manas D, Fox RP, Yeo W, Mo F, Chan AW, Tada T, Iñarrairaegui M, Vogel A, Schweitzer N, Chan SL, Sangro B, Kumada T, Johnson PJ. Long-term impact of liver function on curative therapy for hepatocellular carcinoma: application of the ALBI grade. *Br J Cancer* 2016; **114**: 744-750 [PMID: 27022825 DOI: 10.1038/bjc.2016.33]
8 **Heimbach JK**, Kulik LM, Finn RS, Sirlin CB, Abecassis MM, Roberts LR, Zhu AX, Murad MH, Marrero JA. AASLD guidelines for the treatment of hepatocellular carcinoma. *Hepatology* 2018; **67**: 358-380 [PMID: 28130846 DOI: 10.1002/hep.29086]
9 **Marrero JA**, Kulik LM, Sirlin CB, Zhu AX, Finn RS, Abecassis MM, Roberts LR, Heimbach JK. Diagnosis, Staging, and Management of Hepatocellular Carcinoma: 2018 Practice Guidance by the American Association for the Study of Liver Diseases. *Hepatology* 2018; **68**: 723-750 [PMID: 29624699 DOI: 10.1002/hep.29913]
10 **Lambin P**, Leijenaar RTH, Deist TM, Peerlings J, de Jong EEC, van Timmeren J, Sanduleanu S, Larue RTHM, Even AJG, Jochems A, van Wijk Y, Woodruff H, van Soest J, Lustberg T, Roelofs E, van Elmpt W, Dekker A, Mottaghy FM, Wildberger JE, Walsh S. Radiomics: the bridge between medical imaging and personalized medicine. *Nat Rev Clin Oncol* 2017; **14**: 749-762 [PMID: 28975929 DOI: 10.1038/nrclinonc.2017.141]
11 **Wang F**, Chen Q, Zhang Y, Chen Y, Zhu Y, Zhou W, Liang X, Yang Y, Hu H. CT-Based Radiomics for the Recurrence Prediction of Hepatocellular Carcinoma After Surgical Resection. *J Hepatocell Carcinoma* 2022; **9**: 453-465 [PMID: 35646748 DOI: 10.2147/JHC.S362772]
12 **Wisse E**, De Zanger RB, Charels K, Van Der Smissen P, McCuskey RS. The liver sieve: considerations concerning the structure and function of endothelial fenestrae, the sinusoidal wall and the space of Disse. *Hepatology* 1985; **5**: 683-692 [PMID: 3926620 DOI: 10.1002/hep.1840050427]
13 **Aoki T**, Imamura H, Kaneko J, Sakamoto Y, Matsuyama Y, Kokudo N, Sugawara Y, Makuuchi M. Intraoperative direct measurement of

hepatic arterial buffer response in patients with or without cirrhosis. *Liver Transpl* 2005; **11**: 684-691 [PMID: 15915492 DOI: 10.1002/Lt.20380]

14 **Nardone V**, Reginelli A, Grassi R, Boldrini L, Vacca G, D'Ippolito E, Annunziata S, Farchione A, Belfiore MP, Desideri I, Cappabianca S. Delta radiomics: a systematic review. *Radiol Med* 2021; **126**: 1571-1583 [PMID: 34865190 DOI: 10.1007/s11547-021-01436-7]

15 **Fave X**, Zhang L, Yang J, Mackin D, Balter P, Gomez D, Followill D, Jones AK, Stingo F, Liao Z, Mohan R, Court L. Delta-radiomics features for the prediction of patient outcomes in non-small cell lung cancer. *Sci Rep* 2017; **7**: 588 [PMID: 28373718 DOI: 10.1038/s41598-017-00665-z]

16 **Han X**, Wang M, Zheng Y, Wang N, Wu Y, Ding C, Jia X, Yang R, Geng M, Chen Z, Zhang S, Zhang K, Li Y, Liu J, Gu J, Liao Y, Fan J, Shi H. Delta-radiomics features for predicting the major pathological response to neoadjuvant chemoimmunotherapy in non-small cell lung cancer. *Eur Radiol* 2023 [PMID: 37736804 DOI: 10.1007/s00330-023-10241-x]

17 **Han Z**, Dai H, Chen X, Gao L, Yan C, Ye R, Li Y. Delta-radiomics models based on multi-phase contrast-enhanced magnetic resonance imaging can preoperatively predict glypican-3-positive hepatocellular carcinoma. *Front Physiol* 2023; **14**: 1138239 [PMID: 37601639 DOI: 10.3389/fphys.2023.1138239]

18 **Ji GW**, Zhu FP, Xu Q, Wang K, Wu MY, Tang WW, Li XC, Wang XH. Radiomic Features at Contrast-enhanced CT Predict Recurrence in Early Stage Hepatocellular Carcinoma: A Multi-Institutional Study. *Radiology* 2020; **294**: 568-579 [PMID: 31934830 DOI: 10.1148/radiol.2020191470]

19 **Wen L**, Weng S, Yan C, Ye R, Zhu Y, Zhou L, Gao L, Li Y. A Radiomics Nomogram for Preoperative Prediction of Early Recurrence of Small Hepatocellular Carcinoma After Surgical Resection or Radiofrequency Ablation. *Front Oncol* 2021; **11**: 657039 [PMID: 34026632 DOI: 10.3389/fonc.2021.657039]

20 **Li SQ**, Su LL, Xu TF, Ren LY, Chen DB, Qin WY, Yan XZ, Fan JX, Chen HS, Liao WJ. Radiomics model based on contrast-enhanced computed tomography to predict early recurrence in patients with hepatocellular carcinoma after radical resection. *World J Gastroenterol* 2023; **29**: 4186-4199 [PMID: 37475840 DOI: 10.3748/wjg.v29.i26.4186]

21 **Zhu HB**, Zheng ZY, Zhao H, Zhang J, Zhu H, Li YH, Dong ZY, Xiao LS, Kuang JJ, Zhang XL, Liu L. Radiomics-based nomogram using CT imaging for noninvasive preoperative prediction of early recurrence in patients with hepatocellular carcinoma. *Diagn Interv Radiol* 2020; **26**: 411-419 [PMID: 32490826 DOI: 10.5152/dir.2020.19623]

22 **Li Z**, Yu J, Li Y, Liu Y, Zhang M, Yang H, Du Y. Preoperative Radiomics Nomogram Based on CT Image Predicts Recurrence-Free Survival After Surgical Resection of Hepatocellular Carcinoma. *Acad Radiol* 2023; **30**: 1531-1543 [PMID: 36653278 DOI: 10.1016/j.acra.2022.12.039]

23 **Xu XY**, Ding HG, Li WG, Xu JH, Han Y, Jia JD, Wei L, Duan ZP, Ling-Hu EQ, Zhuang H. Chinese guidelines on the management of liver cirrhosis (abbreviated version). *World J Gastroenterol* 2020; **26**: 7088-7103 [PMID: 33362370 DOI: 10.3748/wjg.v26.i45.7088]

24 **Li W**, Han L, Xiao B, Li X, Ye Z. A Predictive Nomogram of Early Recurrence for Patients with AFP-Negative Hepatocellular Carcinoma Underwent Curative Resection. *Diagnostics (Basel)* 2022; **12** [PMID: 35626229 DOI: 10.3390/diagnostics12051073]

25 **Wei H**, Jiang H, Zheng T, Zhang Z, Yang C, Ye Z, Duan T, Song B. LI-RADS category 5 hepatocellular carcinoma: preoperative gadoxetic acid-enhanced MRI for early recurrence risk stratification after curative resection. *Eur Radiol* 2021; **31**: 2289-2302 [PMID: 33001306 DOI: 10.1007/s00330-020-07303-9]

26 **Xu X**, Zhang HL, Liu QP, Sun SW, Zhang J, Zhu FP, Yang G, Yan X, Zhang YD, Liu XS. Radiomic analysis of contrast-enhanced CT predicts microvascular invasion and outcome in hepatocellular carcinoma. *J Hepatol* 2019; **70**: 1133-1144 [PMID: 30876945 DOI: 10.1016/j.jhep.2019.02.023]

27 **Liu Q**, Li J, Liu F, Yang W, Ding J, Chen W, Wei Y, Li B, Zheng L. A radiomics nomogram for the prediction of overall survival in patients with hepatocellular carcinoma after hepatectomy. *Cancer Imaging* 2020; **20**: 82 [PMID: 33198809 DOI: 10.1186/s40644-020-00360-9]

28 **Zhang XP**, Zhou TF, Wang ZH, Zhang F, Zhong CQ, Hu YR, Wang K, Chai ZT, Chen ZH, Wu MC, Lau WY, Cheng SQ. Association of Preoperative Hypercoagulability with Poor Prognosis in Hepatocellular Carcinoma Patients with Microvascular Invasion After Liver Resection: A Multicenter Study. *Ann Surg Oncol* 2019; **26**: 4117-4125 [PMID: 31321582 DOI: 10.1245/s10434-019-07504-7]

29 **Wu SJ**, Lin YX, Ye H, Xiong XZ, Li FY, Cheng NS. Prognostic value of alkaline phosphatase, gamma-glutamyl transpeptidase and lactate dehydrogenase in hepatocellular carcinoma patients treated with liver resection. *Int J Surg* 2016; **36**: 143-151 [PMID: 27793641 DOI: 10.1016/j.ijsu.2016.10.033]

30 **Dong ZR**, Zou J, Sun D, Shi GM, Ke AW, Cai JB, Sun HC, Qiu SJ, Li T, Zhou J, Zhi XT, Fan J. Preoperative Albumin-Bilirubin Score for Postoperative Solitary Hepatocellular Carcinoma within the Milan Criteria and Child-Pugh A Cirrhosis. *J Cancer* 2017; **8**: 3862-3867 [PMID: 29151974 DOI: 10.7150/jca.21313]

31 **Liu X**, Hou Y, Wang X, Yu L, Jiang L, Yang Z. Machine learning-based development and validation of a scoring system for progression-free survival in liver cancer. *Hepatol Int* 2020; **14**: 567-576 [PMID: 32556865 DOI: 10.1007/s12072-020-10046-w]

32 **Chong HH**, Yang L, Sheng RF, Yu YL, Wu DJ, Rao SX, Yang C, Zeng MS. Multi-scale and multi-parametric radiomics of gadoxetate disodium-enhanced MRI predicts microvascular invasion and outcome in patients with solitary hepatocellular carcinoma ≤ 5 cm. *Eur Radiol* 2021; **31**: 4824-4838 [PMID: 33447861 DOI: 10.1007/s00330-020-07601-2]

33 **Wang F**, Cheng M, Du B, Li LM, Huang WP, Gao JB. Use of radiomics containing an effective peritumoral area to predict early recurrence of solitary hepatocellular carcinoma ≤5 cm in diameter. *Front Oncol* 2022; **12**: 1032115 [PMID: 36387096 DOI: 10.3389/fonc.2022.1032115]

34 **Xia TY**, Zhou ZH, Meng XP, Zha JH, Yu Q, Wang WL, Song Y, Wang YC, Tang TY, Xu J, Zhang T, Long XY, Liang Y, Xiao WB, Ju SH. Predicting Microvascular Invasion in Hepatocellular Carcinoma Using CT-based Radiomics Model. *Radiology* 2023; **307**: e222729 [PMID: 37097141 DOI: 10.1148/radiol.222729]

35 **Liu Y**, Wei X, Zhang X, Pang C, Xia M, Du Y. CT radiomics combined with clinical variables for predicting the overall survival of hepatocellular carcinoma patients after hepatectomy. *Transl Oncol* 2022; **26**: 101536 [PMID: 36115077 DOI: 10.1016/j.tranon.2022.101536]

36 **Kim WJ**, Lim TW, Park PJ, Choi SB, Kim WB. Prognostic markers affecting the early recurrence of hepatocellular carcinoma with liver cirrhosis after curative resection. *Int J Biol Markers* 2019; **34**: 123-131 [PMID: 30977422 DOI: 10.1177/1724600819834306]

37 **Song Y**, Zhou G, Zhou Y, Xu Y, Zhang J, Zhang K, He P, Chen M, Liu Y, Sun J, Hu C, Li M, Liao M, Zhang Y, Liao W. Artificial intelligence CT radiomics to predict early recurrence of intrahepatic cholangiocarcinoma: a multicenter study. *Hepatol Int* 2023; **17**: 1016-1027 [PMID: 36821045 DOI: 10.1007/s12072-023-10487-z]

Published by **Baishideng Publishing Group Inc**
7041 Koll Center Parkway, Suite 160, Pleasanton, CA 94566, USA
Telephone: +1-925-3991568
E-mail: office@baishideng.com
Help Desk: https://www.f6publishing.com/helpdesk
https://www.wjgnet.com